Journal of
Mechanics of
Materials and Structures

A POROELASTIC MODEL FOR CELL CRAWLING INCLUDING MECHANICAL COUPLING BETWEEN CYTOSKELETAL CONTRACTION AND ACTIN POLYMERIZATION

Larry A. Taber, Yunfei Shi, Le Yang and Philip V. Bayly

Volume 6, No. 1-4 January–June 2011

mathematical sciences publishers

JOURNAL OF MECHANICS OF MATERIALS AND STRUCTURES
Vol. 6, No. 1-4, 2011

A POROELASTIC MODEL FOR CELL CRAWLING INCLUDING MECHANICAL COUPLING BETWEEN CYTOSKELETAL CONTRACTION AND ACTIN POLYMERIZATION

LARRY A. TABER, YUNFEI SHI, LE YANG AND PHILIP V. BAYLY

Much is known about the biophysical mechanisms involved in cell crawling, but how these processes are coordinated to produce directed motion is not well understood. Here, we propose a new hypothesis whereby local cytoskeletal contraction generates fluid flow through the lamellipodium, with the pressure at the front of the cell facilitating actin polymerization which pushes the leading edge forward. The contraction, in turn, is regulated by stress in the cytoskeleton. To test this hypothesis, finite element models for a crawling cell are presented. These models are based on nonlinear poroelasticity theory, modified to include the effects of active contraction and growth, which are regulated by mechanical feedback laws. Results from the models agree reasonably well with published experimental data for cell speed, actin flow, and cytoskeletal deformation in migrating fish epidermal keratocytes. The models also suggest that oscillations can occur for certain ranges of parameter values.

1. Introduction

Cell motility plays an important role in many biological processes, including the response to disease and injury, morphogenesis, and the progression of cancer (see [Stossel 1994], for example). Much is known about the molecular and physical mechanisms involved in cell crawling, but how these mechanisms combine to produce directed motion remains incompletely understood. According to the traditional view, cell crawling involves three sequential steps [Flaherty et al. 2007]: (1) actin polymerization pushes a lamellipodium forward from the leading edge; (2) the lamellipodium adheres to the substrate; and (3) cytoskeletal contraction generates tension that breaks weaker adhesions at the rear of the cell and pulls the cell body forward.

Recent work has questioned the order of these events, however, suggesting that contraction precedes polymerization and begins the crawling cycle [Yam et al. 2007; Loitto et al. 2009]. The reason that contraction may be needed to initiate normal cell crawling is unknown. One possibility is that it generates hydrostatic pressure, which helps drive the protrusion at the front of the cell [Charras et al. 2005; Yam et al. 2007]. This idea is a key element of the present study.

The notion that fluid pressure is an important factor in cell crawling is not new. Diffusion alone may not provide a forward flow of actin monomers sufficiently fast to give observed protrusion rates [Oster and Perelson 1987; Zicha et al. 2003], and researchers have speculated that pressure may foster this flow, as well as drive lamellipodial extension [Zhu and Skalak 1988; Stossel 1994; Keren et al. 2009].

Work supported by grants R01 GM075200 and R01 HL083393 from the National Institutes of Health, as well as grant DMS-0540701 from the National Science Foundation.

Keywords: cell migration, poroelasticity, keratocyte.

This idea has fallen out of favor for most cell types, however, as mounting evidence indicates that actin polymerization is the dominant mechanism in lamellipodial extension [Bray 2001]. On the other hand, recent studies have shown that substantial pressure gradients and fluid flow can occur in cells [Charras et al. 2005; Iwasaki and Wang 2008; Mitchison et al. 2008; Keren et al. 2009], suggesting that fluid dynamics may play a larger role in cell motility than commonly thought.

The purpose of this paper is to investigate a new hypothesis for cell crawling that integrates the effects of actin polymerization, cytoskeletal contractility, and intracellular fluid flow. To illustrate the plausibility of our hypothesis, these mechanisms are included in 1-D and 2-D continuum models of a migrating cell. Here, the main focus is on fish epidermal keratocytes, which move relatively quickly (about 0.05–0.2 μm/s) while maintaining a nearly constant shape, in contrast to most other types of cells, which exhibit oscillatory behavior [Bray 2001; Keren et al. 2008]. For realistic parameter values, results from the models agree reasonably well with published experimental data for cell speed, actin flow, and cytoskeletal deformation. In addition, the models predict oscillations (similar to other cell types) for certain parameter values, thereby illuminating some of the inherent feedback control problems that apparently have been solved by crawling keratocytes in order to reach a steady state.

2. Preliminaries

General characteristics of crawling cells. The shape of an epidermal keratocyte (EK) depends on whether it is stationary or crawling, as well as on whether it is located on a 2-D surface or in a 3-D matrix. Stationary cells on a surface resemble the contents of an egg poured onto a flat surface (Figure 1b). The hemispherical yolk in the center corresponds to the cell body, which contains the nucleus and other organelles. The egg white, spread out into a thin disk around the yolk, represents the lamellipodium, which is filled with actin and myosin.

Some cells crawl in a cyclic manner like a worm, e.g., amebas and fibroblasts. They first extend their front end, grab the substrate, and then pull their rear ends forward. In contrast, EKs move more like a centipede, which crawl without changing shape (except to turn). Unlike a centipede, however, EKs

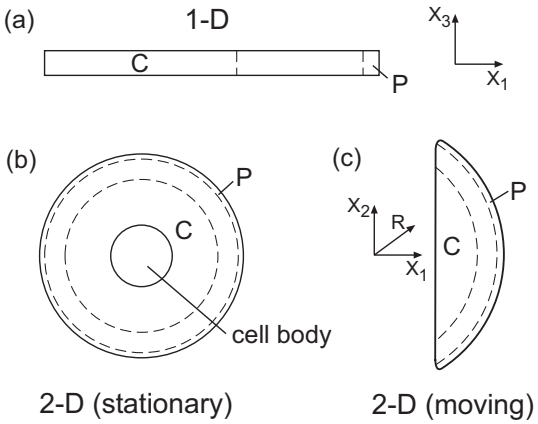

Figure 1. Models for crawling cells (P = actin polymerization zone of lamellipodium; C = CSK contraction zone). (a) 1-D model. (b) Stationary 2-D model. (c) Crawling 2-D model.

apparently are not propelled by dozens of tiny legs. How these cells can crawl steadily at speeds up to 10 μm/min or more is an intriguing and unanswered question.

While crawling on a surface at steady state, the EK lamellipodium becomes shaped like a fan or wing (approximately 40 μm wide, 10 μm long, and 0.2 μm thick; see Figure 1c). Experiments have shown that lamellipodia isolated from the cell body can crawl on their own with a similar speed and shape as intact cells (see Figure 6a) [Verkhovsky et al. 1999]. Hence, this structure is the engine that drives the cell, with the cell body pulled along behind it. The cell body, therefore, can be neglected in models for crawling EKs.

For technical reasons, most experimental studies and models of cell crawling have been two-dimensional. Crawling in three dimensions is quite different, however. For example, cells moving through a 3-D matrix have fewer stress fibers and adhesions, and they must create space in which to move [Friedl and Bröcker 2000]. Moreover, whereas cells on surfaces spread out into a relatively flat configuration, they become spindle shaped as they crawl though tissue. Thus, a 1-D model may be a good approximation for a cell crawling through 3-D tissue.

The cytoskeleton of crawling cells. Cytoskeletal (CSK) dynamics are key to the migration process. Within a relatively narrow region (about 1–2 μm wide) near the leading edge, the lamellipodium is filled with a relatively dense meshwork of branched actin filaments (F-actin). Actin at the front of this region polymerizes to push the cell membrane forward, while actin at the rear depolymerizes into monomers (G-actin), which then move forward to provide a pool for further polymerization. This sets up a treadmilling mechanism [Bray 2001].

Behind this network, F-actin is organized into bundles, and interaction with myosin generates contraction in the crawling direction. Researchers have speculated that this contraction enhances the rate of actin depolymerization and may drive fluid, along with G-actin, toward the leading edge [Svitkina et al. 1997; Zicha et al. 2003; Yam et al. 2007; Keren et al. 2009; Okeyo et al. 2009]. It is notable that actin density decreases and myosin density increases from front to back, and a relatively thick stress fiber forms along the back edge of the lamellipodium.

Proposed crawling mechanism. Combining previous ideas, we herein propose a relatively simple crawling mechanism that integrates the effects of actin polymerization and cytoskeletal contraction. First, CSK contraction elevates the fluid pressure at the rear of the cell, driving fluid (and actin monomers) forward. Next, pressure at the front of the cell pushes the cell membrane forward, creating extra space for monomers and thereby increasing the rate of actin polymerization at the leading edge. Finally, in conjunction with cell-substrate adhesion, the tension generated in the contracting CSK pulls the cell forward.

To achieve steady-state motion, these processes must be continuous and balanced. Hence, coupling between these processes is crucial to the global dynamic behavior of the cell. We suggest that this coupling is regulated by mechanical feedback that depends on the interaction between fluid pressure, CSK stress, and adhesive forces.

3. Governing equations

To model fluid-solid interaction, we take the cytoplasm as a porous elastic material (the CSK) saturated with a viscous fluid, i.e., a poroelastic material. Laying the foundation for the model, this section summarizes the governing equations of nonlinear poroelasticity theory. Then, modifications are discussed for

including growth, which is used to simulate actin polymerization and CSK contraction. The presentation is relatively brief; further details on poroelasticity can be found in [Biot 1972; Kenyon 1976; Yang et al. 1994], while detailed discussions of the growth theory are given, for example, in [Rodriguez et al. 1994; Taber 2001].

Nonlinear poroelasticity theory. In poroelasticity theory, as in the more general mixture theory [Bowen 1976], all points in the bulk material are assumed to be occupied simultaneously by both solid and fluid particles. Here, both the fluid and solid phases are assumed to be incompressible. The total Cauchy stress tensor is given by

$$\boldsymbol{\sigma} = \boldsymbol{\sigma}_s + \boldsymbol{\sigma}_f,$$

where the respective partial stresses of the solid and fluid (per unit area of the bulk material in the current configuration) are

$$\boldsymbol{\sigma}_s = \phi_s \hat{\boldsymbol{\sigma}}_s, \quad \boldsymbol{\sigma}_f = -\phi_f p\, \boldsymbol{I}.$$

In these relations, ϕ_s and ϕ_f are volume fractions, $\hat{\boldsymbol{\sigma}}_s$ is the true solid stress, p is the fluid (pore) pressure, and $\boldsymbol{I}$ is the identity tensor. If there is no mass exchange with the surroundings, $\phi_s + \phi_f = 1$.

Computations are based on a Lagrangian formulation, with all quantities defined relative to the initial (reference) configuration for a cell at rest (taken as stress free). As described below, growth is simulated by introducing an intermediate zero-stress configuration, but we disregard this for the moment. With position vectors to a material point of the solid in the initial and current configurations given by $\boldsymbol{X}$ and $\boldsymbol{x} = \boldsymbol{x}(\boldsymbol{X}, t)$, respectively, the total deformation gradient tensor for the solid skeleton is

$$\boldsymbol{F} = (\nabla \boldsymbol{x})^T, \tag{3-1}$$

where $\nabla \equiv \partial/\partial \boldsymbol{X}$ and superscript T denotes the transpose. The corresponding Lagrange strain tensor is $\boldsymbol{E} = \frac{1}{2}(\boldsymbol{F}^T \cdot \boldsymbol{F} - \boldsymbol{I})$.

The total first Piola–Kirchhoff stress tensor $\boldsymbol{P}$, defined relative to the bulk area in the initial state, is given by [Taber 2004]

$$\boldsymbol{P} = J\boldsymbol{F}^{-1} \cdot \boldsymbol{\sigma}, \tag{3-2}$$

where $J = \det \boldsymbol{F}$ is the dilatation ratio. The equilibrium and constitutive equations can be written in the forms

$$\nabla \cdot \boldsymbol{P} + \boldsymbol{f}_0 = \boldsymbol{0}, \tag{3-3}$$

$$\boldsymbol{P} = \frac{\partial W}{\partial \boldsymbol{F}^T} - Jp\, \boldsymbol{F}^{-1}, \tag{3-4}$$

where $\boldsymbol{f}_0$ and W are the respective body force vector and strain-energy density function per unit bulk reference volume.

Fluid flow is governed by a generalized Darcy's law of the form [Yang et al. 1994]

$$\dot{\boldsymbol{U}} = -\boldsymbol{K} \cdot \nabla p, \tag{3-5}$$

where $\dot{\boldsymbol{U}}$ is the volume flow rate of fluid relative to the solid, per unit bulk material area in the reference state, and dot denotes time differentiation. In terms of $\dot{\boldsymbol{U}}$, the relative fluid velocity is $\boldsymbol{v}_f = J^{-1}\dot{\boldsymbol{U}} \cdot \boldsymbol{F}^T$. In addition,

$$\boldsymbol{K} = \boldsymbol{F}^{-1} \cdot \boldsymbol{k} \cdot \boldsymbol{F}^{-T} J/\mu_f$$

is the effective permeability tensor, with $\boldsymbol{k}$ being the intrinsic permeability tensor and μ_f the fluid viscosity.

Finally, for incompressible fluid and solid constituents, equating the net volume flow rate of fluid entering a material element to the rate of change of element volume gives the incompressibility (continuity) condition

$$-\nabla \cdot \dot{\boldsymbol{U}} = \dot{J}.$$

This equation can be integrated to yield

$$\nabla \cdot \boldsymbol{U} + J - 1 = 0. \tag{3-6}$$

Given appropriate boundary and initial conditions, equations (3-1), (3-3), (3-4), (3-5) and (3-6) can be solved for $\boldsymbol{x}$, $\boldsymbol{F}$, $\boldsymbol{P}$, $\boldsymbol{U}$, and p. Note that if $\boldsymbol{K} = \boldsymbol{0}$, then $\boldsymbol{U} = \boldsymbol{0}$ and these equations reduce to the governing equations for an incompressible solid, with p becoming a Lagrange multiplier [Taber 2004].

Growth. Polymerization and contraction are simulated using a theory for volumetric growth of an elastic solid [Rodriguez et al. 1994; Taber 2001]. Positive growth along an actin fiber simulates polymerization, while negative growth simulates contraction.

In this theory, the growth tensor $\boldsymbol{G}$ transforms the zero-stress reference state for each material element into an intermediate (virtual) zero-stress state of different size and shape. Geometric compatibility between growing elements is ensured by the elastic deformation gradient tensor $\boldsymbol{F}^*$, and the total deformation gradient tensor is written is the form

$$\boldsymbol{F} = \boldsymbol{F}^* \cdot \boldsymbol{G}. \tag{3-7}$$

With this formulation, growth occurs relative to the reference configuration. In addition, stress depends only on $\boldsymbol{F}^*$, and the Cauchy stress tensor is given by [Taber 2001]

$$\boldsymbol{\sigma} = J^{*-1} \boldsymbol{F}^* \cdot \frac{\partial W}{\partial \boldsymbol{E}^*} \cdot \boldsymbol{F}^{*T} - p\, \boldsymbol{I}, \tag{3-8}$$

from which (3-2) provides $\boldsymbol{P}$. In the resulting expression, which replaces (3-4), $J^* = \det \boldsymbol{F}^*$, $W = W(\boldsymbol{E}^*)$, and $\boldsymbol{E}^* = \frac{1}{2}(\boldsymbol{F}^{*T} \cdot \boldsymbol{F}^* - \boldsymbol{I})$.

In our models, the growth tensor is determined by mechanical feedback laws. These laws have the general rate form $\dot{\boldsymbol{G}} = \dot{\boldsymbol{G}}(\boldsymbol{X}, t; \boldsymbol{F}; \hat{\boldsymbol{\sigma}}_s, p)$, which is specialized below.

4. Proposed models for cell crawling

In this paper, we present 1-D and 2-D poroelastic models for a cell crawling on a flat surface S. To define the geometry, let X_i represent a Cartesian coordinate system fixed to S, with X_1 directed along the crawling direction and X_3 normal to S.

Geometry and material properties. The 1-D model represents a narrow strip along the centerline of the lamellipodium in the X_1-X_3 plane. In the initial resting state, the cell is taken as a rectangular bar (or plate) of length 10 μm and height 1 μm (Figure 1a). This model also can be considered a first approximation for a spindle-shaped cell crawling through a 3-D matrix. (The cell height, which is

irrelevant in the present study, is taken unrealistically large to improve numerical convergence in the 1-D model.)

The 2-D model represents an EK lamellipodium in the X_1-X_2 plane. The stationary lamellipodium is taken as a circular annulus of outer radius 10 μm surrounding a cell body of radius 3 μm (Figure 1b). For a crawling cell, the lamellipodium initially has the shape of a section of a circle with rounded corners and approximately the same planform area as the lamellipodium in the stationary model (Figure 1c); the cell body is not included. For convenience, the center of the circle defining the leading edge at $t = 0$ is placed at the origin of the X_i system.

Actually, both models are analyzed as two-dimensional objects, just in different planes, with the 1-D and 2-D models assumed to be under conditions of plane strain and plane stress, respectively. The cell membrane is not included explicitly, but the boundaries are assumed to be impermeable to flow. Hence, the total cell volume remains constant, although fluid can flow from one region to another.

The strain-energy density function for the solid skeleton must have a compressible form. For a first approximation, we assume that the CSK is transversely isotropic and take

$$W = C\left[I^* - 3 + \frac{1-2\nu}{\nu}\left(J^{*\,-2\nu/(1-2\nu)} - 1\right)\right] + C_3 E_{33}^{*2}, \tag{4-1}$$

where the term in brackets corresponds to a Blatz–Ko material [1962] and the last term provides a stiffening in the X_3-direction that prevents the lamellipodium from thickening unrealistically during crawling. We speculate that relatively short and stiff crosslinks between actin filaments, as well as connections between actin and the cell membrane, provide this additional transverse stiffness. The parameters C and ν represent the small-strain modulus and Poisson's ratio, respectively, of the drained solid skeleton, C_3 is the transverse modulus, and $I^* = \mathrm{tr}\,(\boldsymbol{I} + 2\boldsymbol{E}^*)$ is a strain invariant.

Actin polymerization. Polymerization of actin filaments is simulated by growth of the solid skeleton in a narrow zone near the leading edge of the model, along the local fiber coordinate (X_f) normal to the edge in the reference configuration. In the 1-D model, X_f is the longitudinal coordinate X_1, whereas in the 2-D models, it is the radial direction R (Figure 1b,c). Since growth in our models is one-dimensional, the growth tensor $\boldsymbol{G}$ has only one non-zero component, denoted here simply by G. With the initial value of G set to unity everywhere, $G > 1$ gives polymerization and $G < 1$ gives contraction (see below).

It is important to note that simulating actin polymerization by volumetric growth of filaments is a relatively crude approximation for the actual process. At the molecular level, the addition of monomers to the end of a filament actually is a type of surface growth. To more accurately model polymerization in a continuum formulation, a multiscale analysis is needed. This would be a natural extension of the present model.

Feedback control of polymerization in the models is based on the work of Peskin et al. [1993], who postulate that, at the leading edge of a crawling cell, actin filaments push the cell membrane forward via a Brownian ratchet mechanism. According to this idea, thermal fluctuations in the membrane create a small gap between the membrane and actin filaments, allowing actin monomers to enter and add to the length of the filaments. Here, we propose that positive fluid pressure at the leading edge facilitates this process by pushing the cell membrane forward, enlarging the gap and increasing the rate of polymerization. This

mechanism is implemented through the feedback law

$$\ddot{G}_p = A_p\, \dot{p}_L\, g_p(x_f), \tag{4-2}$$

where G_p represents the growth due to polymerization, p_L is the fluid pressure at the leading edge, and A_p is a positive rate constant. With this law taken as second order in time, the polymerization rate ($\dot{G}_p$) becomes constant when pressure reaches a steady state ($\dot{p}_L = 0$).

In the equation above, the function g_p provides the spatial distribution of growth in the current configuration. With x_L denoting the current location of the leading edge, we take

$$g_p(x_f) = H_s(x_f - (x_L - \Delta x_p, \Delta x_{jp}))(1 - \beta X_2^2), \tag{4-3}$$

in which H_s is a smoothed Heaviside step function defined in the region $x_f \geq x_L - \Delta x_p$. In this expression, x_f is the local fiber coordinate (the growth direction), Δx_p defines the (specified) width of the growth zone, and Δx_{jp} is the length of the smoothed "jump" from zero to one. This form for g_p keeps the width of the active polymerization zone fixed in the crawling direction, rather than growing longer with G. In addition, the term with the specified constant β allows for a gradient in polymerization force along the leading edge of the 2-D crawling model ($g_c = 0$ for $|X_2| > 1/\sqrt{\beta}$ and $\beta = 0$ for the 1-D and 2-D stationary models). Some investigators have speculated that the observed regional variation in actin density, being highest near the center and lowest near the sides of the cell, plays an important role in maintaining cell shape [Keren et al. 2008; Rubinstein et al. 2009].

Cytoskeletal contraction. Actomyosin contraction occurs in a wider zone toward the back of the cell [Yam et al. 2007]. To achieve steady-state conditions, we speculate that the contraction is continuous in time, i.e., the contracting region never relaxes. For this to occur, contraction is assumed to be accompanied by CSK remodeling, similar to the contractile mechanism of smooth muscle [An and Fredberg 2007; Bossé et al. 2008]. As a smooth muscle cell contracts, its CSK remodels to reset the zero-stress configuration so that shortening can continue to very large magnitudes. This process is included in the present models by progressively enlarging the contractile region so it maintains a constant width as it contracts. In the 1-D and stationary 2-D models, contraction is assumed to occur in the same direction as actin polymerization, i.e., normal to the leading edge. In the 2-D crawling model, contraction occurs in the direction of motion.

To obtain steady-state motion, feedback is included in the contractile machinery. A growing amount of evidence suggests that cells and tissues respond to mechanical perturbations in ways that tend to restore a homeostatic state of stress [Humphrey 2008]. Correspondingly, we assume that a homeostatic (target) stress $\hat{\sigma}_0$ exists for contractile fibers and propose a contraction feedback law of the form

$$\ddot{G}_c = -A_c^2(1 - \hat{\sigma}_s/\hat{\sigma}_0)g_c(x_f), \tag{4-4}$$

where G_c is the (negative) growth due to contraction, $\hat{\sigma}_s$ is the true solid stress in the fiber direction, and A_c is a rate constant. With this law, the contractile rate ($\dot{G}_c$) becomes constant when $\hat{\sigma}_s = \hat{\sigma}_0$.

The spatial distribution for contraction is taken in a form similar to that given above for g_p, i.e.,

$$g_c = [1 - H_s(x_f - (x_0 + \Delta x_c, \Delta x_{jc}))](1 - \beta X_2^2), \tag{4-5}$$

where x_0 is the current location of the trailing edge of the lamellipodium, and the lengths Δx_c and Δx_{jc} provide an active contractile zone of constant geometry in the current configuration. In the axisymmetric model for a stationary cell, we take $\beta = 0$, as well as $g_c = 0$ in the cell body (Figure 1b).

Once G_p and G_c are computed, the total growth is given by $G = G_p G_c$.

Adhesion dynamics. Adhesion between the CSK and the substrate is modeled by a frictional body force [Alt and Dembo 1999; Gracheva and Othmer 2004; Kruse et al. 2006; Kuusela and Alt 2009]. The proportionality between velocity and force represents the cumulative effects of a number of adhesions. The force on each adhesion depends on the displacement of the cytoskeleton relative to the undeformed substrate, over the time since the adhesion was formed. If adhesion lifetime is approximately constant, net adhesion force will increase roughly in proportion to velocity, and the coefficient in this relationship will increase with density of adhesions, adhesion stiffness, and substrate stiffness. Other dissipative forces, such as those caused by viscous resistance between the CSK and cell membrane, as well as between the cell membrane and the surrounding environment, are included through an additional friction force. The total friction force is given by

$$\boldsymbol{f}_0 = -\eta \boldsymbol{v}_s - \eta_c \boldsymbol{v}_c, \tag{4-6}$$

where η and η_c are friction coefficients for the adhesions and cell membrane interaction, respectively. In addition, $\boldsymbol{v}_s$ is the local velocity vector for the solid skeleton (CSK), and $\boldsymbol{v}_c$ is the forward velocity of the cell as a whole, taken as the velocity at the center of the leading edge.

5. Computational methods

To express the governing equations in dimensionless form, the following nondimensional variables are defined:

$$\bar{\boldsymbol{X}} = \frac{\boldsymbol{X}}{L}, \quad \bar{\boldsymbol{x}} = \frac{\boldsymbol{x}}{L}, \quad \bar{\nabla} = L\nabla, \quad \bar{t} = \frac{t}{T}, \quad \bar{U} = \frac{U}{L}, \quad \bar{\boldsymbol{v}} = \frac{\boldsymbol{v}T}{L},$$

$$\bar{\boldsymbol{\sigma}} = \frac{\boldsymbol{\sigma}}{C}, \quad \bar{\boldsymbol{P}} = \frac{\boldsymbol{P}}{C}, \quad \bar{\boldsymbol{f}}_0 = \frac{\boldsymbol{f}_0 L}{C}, \quad \bar{p} = \frac{p}{C}, \quad \bar{W} = \frac{W}{C}, \quad \bar{C}_3 = \frac{C_3}{C},$$

$$\bar{K} = \frac{CT}{L^2} K, \quad \bar{\eta} = \frac{L^2}{CT} \eta, \quad \bar{A}_p = CT A_p, \quad \bar{A}_c = T A_c.$$

The characteristic length L is taken as the initial cell length ($10\,\mu$m), and the characteristic time is defined as $T = L/v_c = 50$ s for a cell velocity $v_c = 0.2\,\mu$m/s. Thus, it typically takes an EK about 50 s to move a distance equal to its own length. In terms of these quantities, the governing equations (3-1), (3-3), (3-5), (3-6), (3-8), (4-2), (4-4), and (4-6) maintain their dimensional forms if we let dot denote $d/d\bar{t}$ and remove all bars. Unless stated otherwise, all results are given in terms of nondimensional variables with the bars implied.

Finite element modeling. Finite element models were developed using the commercial software Comsol Multiphysics (v. 3.5; Comsol AB, Burlington, MA). The Structural Mechanics Module provided the basis for the nonlinear elastic part of the model. The governing equations were modified to implement volumetric growth as described in [Taber 2008], with Darcy's law and the feedback laws included as auxiliary differential equations. In addition, the following changes were made to enforce incompressibility:

- The extra term $-p\,\delta$ was added to the strain-energy density function, where δ is the expression on the left side of (3-6) and p is a Lagrange multiplier with the physical meaning of fluid pressure.
- The expression $(p/M+\delta)p_t$ was included as a weak constraint condition, where p_t is a test function and M is a (large) penalty parameter (set to 10^5).

Triangular second-order and first-order elements were used for displacement (solid elasticity) and pressure (fluid flow), respectively. The mesh was refined until the model yielded sufficient solution accuracy. The function *flc2hs* provided the smoothed Heaviside function used in the feedback laws.

Finally, we note that the model is unstable when it is required to meet the target stress at all points in the CSK. To improve stability, we used the average value of the true solid stress over the rear $4\,\mu$m (1-D and 2-D crawling models) or $3\,\mu$m (2-D stationary model) along the cell centerline for $\hat{\sigma}_s$ in (4-4). Testing showed that the length of the averaging region has a relatively small impact on the results. Similarly, the value of p_L in (4-2) was taken at the middle of the leading edge.

Simulation procedure. Initially, the model is at rest with no stresses and $\boldsymbol{G}=\boldsymbol{I}$. All boundaries are stress free and impermeable to flow ($\boldsymbol{P}\cdot\boldsymbol{N}=\dot{\boldsymbol{U}}\cdot\boldsymbol{N}=0$, where $\boldsymbol{N}$ is the local normal to the boundary in the reference configuration). There are no specified loads or displacements. At the outset of the simulation, the feedback law (4-4) initiates a contraction at the rear of the cell, generating fluid pressure, and the other feedback law (4-2) causes growth near the front that pushes the leading edge forward. Except for time plots and results from the 2-D crawling model, all results are plotted after the cell reaches steady-state conditions.

Parameter values. The geometries of the polymerization and contraction zones were estimated from published distributions of F-actin, myosin II, and contractile strains in crawling EKs [Svitkina et al. 1997; Adachi et al. 2009]. The values used in the models are $\Delta x_p=\Delta x_{jp}=1\,\mu$m, $\Delta x_c=4\,\mu$m (1-D & 2-D crawling) or $2\,\mu$m (2-D stationary), $\Delta x_{jc}=4\,\mu$m (1-D & 2-D crawling) or $3\,\mu$m (2-D stationary), and $\beta=0.25$.

Otherwise, with $\boldsymbol{K}=K\boldsymbol{I}$ (isotropic permeability), the models contain ten physical parameters: C, C_3, ν, K, ϕ_s ($\phi_f=1-\phi_s$), η, η_c, A_p, A_c, and $\hat{\sigma}_0$. Unfortunately the range of reported parameter values is quite large in some cases. For example, estimates for the hydraulic permeability (K) range over at least five orders of magnitude, from about 10^{-10} to 10^{-15} m^4/N s [Guilak et al. 2006]. Hence, after first obtaining first-approximation parameter values from published data as described below, we iteratively correlated model and experimental results to refine these values in order to define a baseline model (Table 1). We also used this method to guide our choices for the functions g_p and g_c in (4-2) and (4-4).

In defining the mechanical properties of the cytoskeleton, we note that recent studies have shown that the CSK is capable of very rapid remodeling [An and Fredberg 2007; Bossé et al. 2008]. Hence, we assume that CSK remodeling keeps up with the dynamics of the crawling cell and take the porosity and permeability as constant. The representative values $\phi_s=\phi_f=0.5$ are used for the volume fractions, and the value taken for K is near the low end of the range given above (Table 1). The values chosen for C and ν are typical for a compressible cell [Guilak et al. 2006], while C_3 is taken large enough to prevent significant changes in lamellipodium thickness.

Parameter	Physical meaning	Value	Nondimensional Value
C	CSK modulus	1 kPa	1
C_3	Transverse fiber modulus	20 kPa	20
ν	Poisson's ratio	0.3	0.3
K	Effective hydraulic permeability	4×10^{-15} m^4/N s	2
η	Adhesion friction coefficient	200 Pa s/μm^2	0.4
η_c	Cell membrane friction coefficient	50 Pa s/μm^2	0.1
A_p	Actin polymerization rate constant	1 (kPa s)$^{-1}$	50
A_c	CSK contraction rate constant	0.2 s^{-1}	10
$\hat{\sigma}_0$	Target stress	0.5 kPa	0.5

Table 1. Parameter values for baseline model.

The value used for the friction coefficient (η) was measured by [Fournier et al. 2010]. The membrane friction coefficient (η_c) is assumed to be similar to η, but smaller to keep the cell moving forward.

The rate constants (A_p and A_c) and the target stress ($\hat{\sigma}_0$) were estimated as follows. The value of $\hat{\sigma}_0$ is based on measurements of actomyosin contractile stress (~ 0.4 kPa) in EKs [Galbraith and Sheetz 1999]. The constant A_c in (4-4) characterizes the rate of contraction under zero load conditions. With the unloaded speed of myosin relative to actin being approximately $v_m = 6\,\mu$m/s [Howard 2001], the fractional contraction rate is roughly $A_c = v_m/\Delta x_c \cong 1.5\,\text{s}^{-1}$, but we ended up using a somewhat smaller value (Table 1).

Finally, to estimate the actin polymerization rate constant A_p, we use two pieces of information: (1) the unloaded polymerization velocity for actin is approximately $v_0 = 0.8\,\mu$m/s [Peskin et al. 1993]; and (2) the stall stress for actin polymerization is about $\sigma_s = 2$ kPa in EKs [Prass et al. 2006]. Then, taking the force-velocity relation as linear (a very rough approximation) yields $A_p = (v_0/\Delta x_p)/\sigma_s = 0.4$ (kPa s)$^{-1}$.

Again, all of these values were modified somewhat to obtain more accurate model behavior, and, unless stated otherwise, the results for both the 1-D and 2-D models are based on the parameters given in Table 1. Because of incomplete and inconsistent data, it was important to conduct a parametric sensitivity analysis (see Results section).

6. Results

One-dimensional model. Steady-state distributions along the cell are shown for actin velocity ($v_s = \dot{x}_1$), CSK stretch rate ($\dot{F}_{11}$), actin stress ($\hat{\sigma}_s$), fluid pressure (p), and relative fluid velocity (v_f) (Figure 2). For clarity, except in the plots of the deformed cell (Figure 2a), all quantities are plotted as functions of the undeformed coordinate X_1. To illustrate the effects of fluid flow, curves are shown for various values of the effective hydraulic permeability K.

Actin velocity is forward at the front and back of the cell, but backward elsewhere (Figure 2b). The retrograde flow of actin is caused by growing actin filaments at the front pushing backwards as they meet frictional resistance to forward motion (due to adhesions). The magnitude of the actin velocity increases with K in each region.

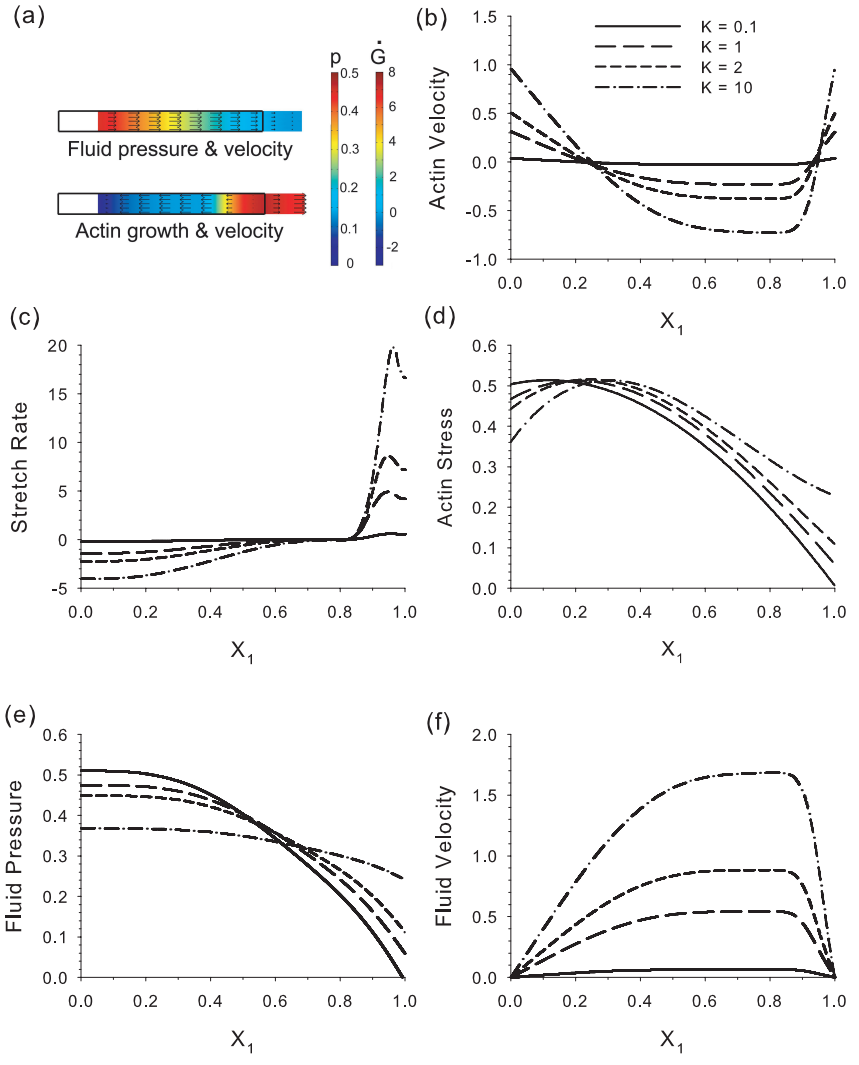

Figure 2. Steady-state distributions in 1-D model. Except in (a), quantities are plotted as functions of the undeformed longitudinal coordinate. Results are shown for various values of the effective hydraulic permeability K, with $K = 2$ giving the baseline case and the legend in (b) applying to all plots. (a) Deformed cell geometry (outline is initial geometry). Top: pressure (colors) and relative fluid velocity (arrows); bottom: growth rate (colors) and actin velocity (arrows). (b) Actin velocity. (c) Stretch rate. (d) Actin (solid) stress. (e) Fluid pressure. (f) Relative fluid velocity.

Actin polymerization causes a positive stretch rate near the leading edge, while CSK contraction generates increasingly negative stretch rates toward the rear (Figure 2c). The stretch-rate magnitudes increase with K. In addition, the actin (solid) stress distribution peaks near the rear of the cell and drops off toward the front (Figure 2d).

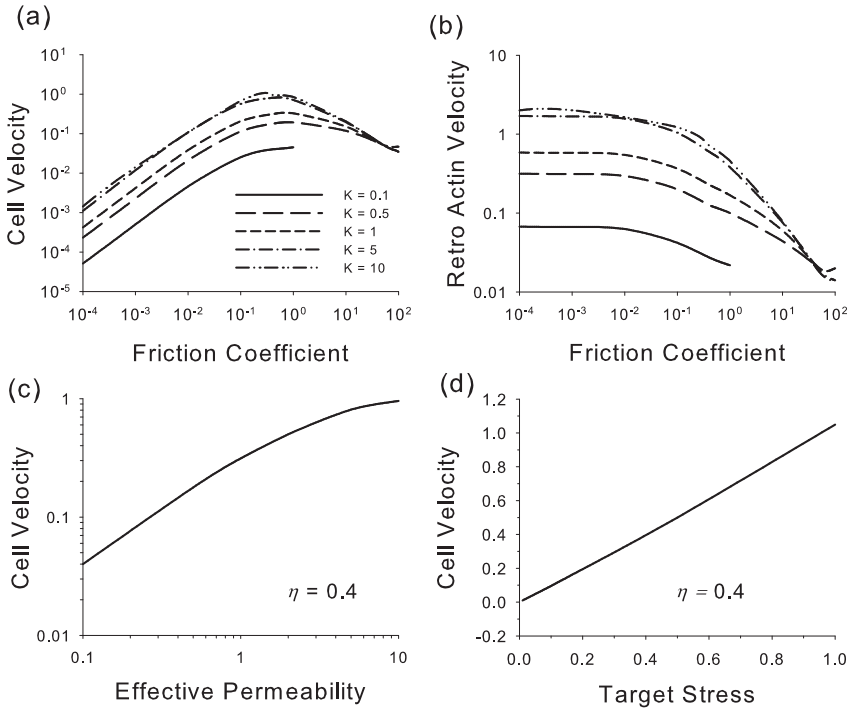

Figure 3. Effects of adhesiveness (friction) and target stress on cell velocity and retrograde actin flow in 1-D model. (a) Cell velocity vs friction coefficient η for various values of effective hydraulic permeability K. (b) Retrograde actin velocity vs η for various K (same legend as in (a)). (c) Cell velocity vs K for $\eta = 0.4$. (d) Cell velocity vs target stress $\hat{\sigma}_0$ for $\eta = 0.4$.

The fluid pressure is positive throughout the cell (Figure 2e). It is greatest at the trailing edge and decreases to a minimum at the leading edge. The negative pressure gradient, which is produced by the combined effects of contraction at the rear and growth at the front, drives the fluid forward. The fluid velocity relative to the solid skeleton peaks near the leading edge and meets the boundary conditions of zero relative flow at the front and back (Figure 2f). Although the pressure gradient decreases with increasing values of K (Figure 2e), the fluid velocity increases because the higher permeability offers less resistance to flow.

Cell speed (actin speed at the leading/trailing edge) depends in a biphasic manner on adhesiveness, as represented by the friction coefficient η (Figure 3a). It is small at low and high values of η and reaches a peak between $\eta = 0.1$ and 1. In contrast, the retrograde actin velocity is nearly constant for $\eta < 0.01$ but drops off for larger values of η (Figure 3b). For the baseline value $\eta = 0.4$, cell speed increases with K and approaches a constant value for $K > 10$ (Figure 3c). However, the speed increases in proportion to the target stress $\hat{\sigma}_0$ over the range of values studied (Figure 3d).

Finally, results are presented to illustrate the temporal behavior of the model. At the beginning of the simulation, the start-up conditions produce oscillations which eventually damp out in most cases, leaving

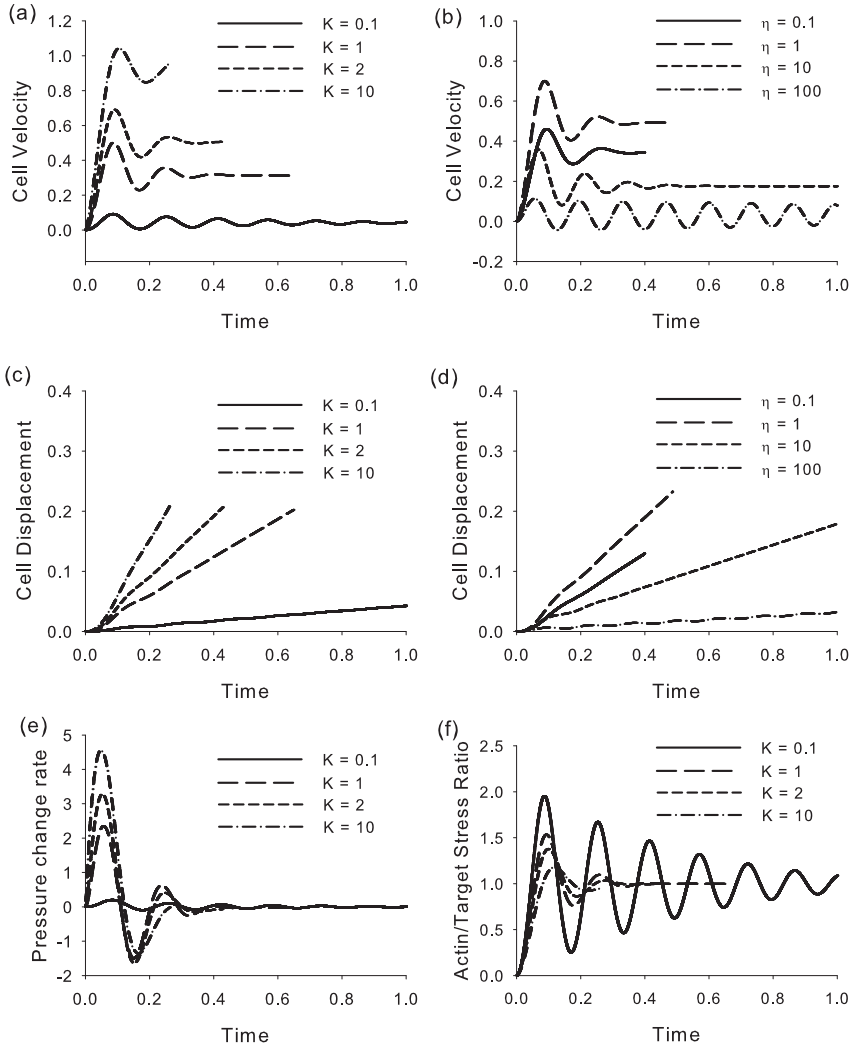

Figure 4. Time-dependent behavior of 1-D model. (a) Cell velocity for various values of the effective hydraulic permeability K. (b) Cell velocity for various values of the friction coefficient η. (c) Cell displacement for various K. (d) Cell displacement for various η. (e) Rate of change in fluid pressure for various K. (f) Ratio of actin (solid) stress to target stress ($\hat{\sigma}_s/\hat{\sigma}_0$) for various K.

a steady-state condition (Figure 4a,b). At steady state, the fluid pressure becomes constant and $\hat{\sigma}_s \to \hat{\sigma}_0$ (Figure 4e,f).

For certain parameter values, however, the oscillations persist and may continue indefinitely. We found that this behavior is especially sensitive to the values of K and η, as persistent oscillations appear for low values of K and high values of η (Figure 4a,b). Even when cell speed oscillates, however, the net motion is forward in all cases (Figure 4c,d).

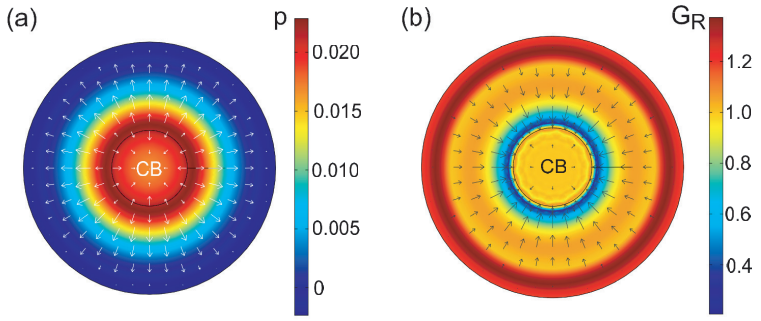

Figure 5. Results for stationary 2-D model ($t = 0.45$; CB = cell body). (a) Pressure (colors) and relative fluid velocity (arrows). (b) Radial growth (colors) and actin velocity (arrows).

Two-dimensional model. Unfortunately, the present 2-D models do not reach steady state. (A parameter study failed to find a suitable combination of parameter values.) Hence, we present only illustrative results at times when nearly steady-state conditions occur.

Although the fluid pressure in the stationary model is relatively small, the pressure gradient is significant enough to drive fluid radially outward from the cell body everywhere except near the leading edge and within the cell body (Figure 5a). At the same time, the actin CSK flows inward throughout the lamellipodium except for a small outward motion due to polymerization near the outer edge (Figure 5b).

The crawling model acquires the characteristic fan-like shape of an EK (Figure 6). Near the symmetry axis of the cell, the results are similar to those from the 1-D model. In particular, a pressure gradient drives fluid toward the leading edge (Figure 6b), while actin flows backward in the middle of the cell and forward near the front and back edges (Figure 6c). Near the tips of the "wing," however, relatively little fluid flow occurs, but the actin moves radially inward at considerable speed. The continued lateral deformation is one reason for the failure to achieve steady state. Also shown is a map of the frictional body force exerted by adhesions on the cell (Figure 6d). Peaks in force occur near the front and back edges, with strong concentrations at the wing tips.

7. Discussion

Theoretical modeling has played a central role in studies of cell migration. Models promote understanding of the physical processes underlying observed behavior. They also can be used to test whether a given hypothetical mechanism is consistent with physical law.

Previous models for cell crawling. Here, we provide a brief summary of some of the models most pertinent to the present work, focusing primarily on 1-D and 2-D models with a significant mechanical component. More comprehensive recent reviews of this topic include those of [Flaherty et al. 2007; Carlsson and Sept 2008].

DiMilla et al. [1991] proposed one of the first models for cell crawling that includes adhesion dynamics. The CSK is modeled as a 1-D viscoelastic system of springs and dashpots, with contractile elements providing the driving force, which mediates binding affinities. Notably, this model predicts the experimentally observed biphasic behavior of cell speed with increasing substrate adhesiveness. In particular,

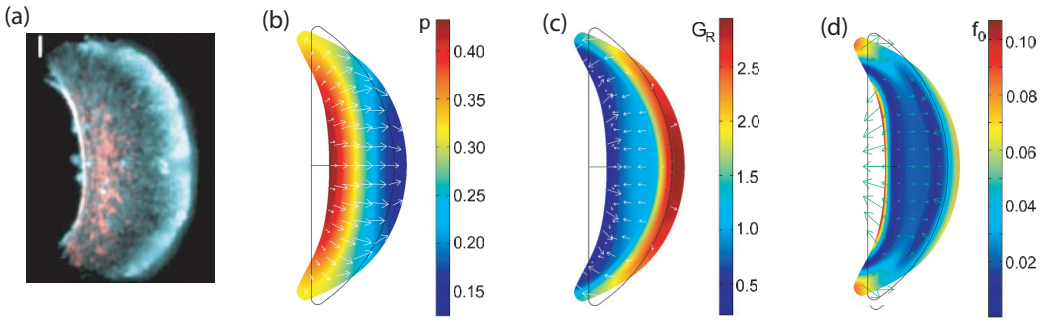

Figure 6. Results for 2-D model crawling toward the right ($t = 0.3$; outlines indicate initial configuration). (a) Image of isolated EK lamellipodium crawling on a surface (red: myosin II; cyan: actin) (reprinted with permission from [Verkhovsky et al. 1999]). (b) Pressure (colors) and relative fluid velocity (arrows). (c) Radial growth (colors) and actin velocity (arrows). (d) Frictional body force (colors and arrows) exerted by substrate on the cell.

cell speed is low for either very high or very low adhesiveness, and it peaks at some intermediate value [Palecek et al. 1997]. A common interpretation for this behavior is that cells cannot gain enough traction to move quickly on very slippery surfaces, while they have difficulty letting go of very sticky surfaces [DiMilla et al. 1991]. The present model captures this fundamental behavior (Figure 3a).

In [Alt and Dembo 1999; Kuusela and Alt 2009] the cytoplasm is treated as a biphasic fluid-like mixture. One phase contains actin and myosin filaments, and the other phase is a solvent containing actin monomers. The phases exchange monomers through chemical reactions, and the forces of actin polymerization and CSK contraction are simulated by positive and negative pressures, respectively. Other investigators also have considered the cytoplasm as a fluid-like mixture (e.g., [Kruse et al. 2006; Rubinstein et al. 2009].

Modeling the CSK as a fluid is based on the argument that the time scales for CSK remodeling and function are similar [Alt and Dembo 1999]. At low Reynolds numbers like those in a cell, however, fluid stress is dominated by pressure, which is intrinsically isotropic, whereas solid-like behavior is needed to produce directed (anisotropic) stress like that generated by actin polymerization and CSK contraction. Our model includes rapid remodeling of contractile fibers, but they are considered as elastic solids.

Hydrostatic pressure provides the driving force in some published models for pseudopod extension and blebbing [Young and Mitran 2010; Oster and Perelson 1987]. In our model, pressure plays a central but more indirect role, as it modulates the rate of actin polymerization at the leading edge, but actin filaments do the actual "pushing." The pseudopod extension model of [Zhu and Skalak 1988] is similar in some respects to our model. In their model, actin polymerization pushes the cell membrane forward, creating a pressure drop that draws fluid and actin monomers toward the leading edge. As in the present model, fluid flow is governed by Darcy's law.

Stolarska et al. [2009] presented a 3-D finite element model for an EK crawling on a surface. The cell is treated as a viscoelastic solid, and focal adhesions are included at the boundary with the substrate. As in our model, actin polymerization and CSK contraction are simulated using volumetric growth. However, growth is specified in their model, rather than being governed by feedback.

The 1-D model of [Larripa and Mogilner 2006] treats the cell as a viscoelastic actin-myosin gel. Contractile stress is assumed to be proportional to the concentration of myosin bound to actin, as computed from chemical kinetics. This model achieves steady-state motion like an EK.

Perhaps the most biochemically comprehensive model for a crawling cell is the 2-D model of [Rubinstein et al. 2005] for an EK lamellipodium. This model includes turnover of actin and actomyosin fibers, forces generated by actin polymerization and actomyosin contraction, and actin transport. External loads and displacements are applied at the boundaries in an ad hoc manner, whereas all loads in our models arise automatically from mechanical feedback.

Comparison of numerical and experimental results. A theoretical model is only as good as the experimental data used to support and test it. Over the years, numerous experimental studies of cell crawling have been published. Many of these studies have been qualitative, but recent reports have emphasized quantitative measurements. We used some of these data to estimate parameter values for our models, but, as noted above, the available data are not always consistent. In addition to natural biological variability, the use of different cell and substrate types contribute to this inconsistency. Nevertheless, it is important to compare numerical and experimental results when possible.

In general, results given by previous models for cell crawling have been compared with only limited portions of the available experimental data. Here, we evaluate our models using the following data for EKs under steady-state conditions:

(1) The speed and shape of a crawling EK are relatively constant. At steady state, our 1-D model is consistent with this observation. The steady-state cell speed in the 1-D baseline model is approximately 0.1 μm/s, which is within the range of reported values (about 0.05–0.2 μm/s; see, e.g., [Adachi et al. 2009; Okeyo et al. 2009; Wilson et al. 2010]. The speed is similar in the 2-D model, but this model does not achieve steady state.

(2) As discussed above, cell speed depends on adhesion strength in a biphasic manner. (Actually, this behavior has been found in at least two cell types [Palecek et al. 1997; Peyton and Putnam 2005]; to our knowledge this effect has not been explored in EKs.) Our 1-D model captures this behavior, including the shapes of the cell velocity vs adhesiveness (η) curves and the result that cell velocity increases by approximately an order of magnitude for a similar increase in adhesiveness (Figure 3a).

(3) In crawling cells, the actin CSK moves forward relative to the substrate at the front and back of the lamellipodium and backwards in between [Schaub et al. 2007; Yam et al. 2007; Fournier et al. 2010]. In stationary (circular) EKs, on the other hand, actin flows radially inward toward the cell body throughout the lamellipodium [Yam et al. 2007]. Both the 1-D and 2-D models are consistent with these results (Figures 2a,b and 5b). In the 1-D baseline model, the retrograde actin speed is about 0.07 μm/s, which is similar to measured values for EKs [Schaub et al. 2007; Adachi et al. 2009].

(4) In the direction of motion, strain rate along the midline of the lamellipodium is positive near the leading edge and negative toward the rear [Adachi et al. 2009]. Results from our models are consistent with this pattern (Figure 2c). In addition, the magnitude of the peak negative strain rate in the 1-D baseline model is about $-0.04\ \mathrm{s}^{-1}$, which is nearly the same as that measured in EKs by Adachi et al.

(5) Relative to the CSK, intracellular fluid flows forward through the lamellipodium [Keren et al. 2009]. Both the 1-D and 2-D models give this result (Figures 2f and 6b). However, the fluid and solid velocities in our models are similar, whereas Keren at al. found that relative fluid velocity is about 40% that of the cell.

(6) The largest traction stresses between a crawling EK and the substrate occur along the leading and trailing edges of the cell, as well as near the tips of the "wings" [Jurado et al. 2005; Fournier et al. 2010]. Our 2-D model is consistent with these data, including the result that the maximum traction occurs at the wing tips (Figure 6d), but the measured traction direction at the tips is opposite to that predicted by the model.

(7) According to our 1-D model, cell velocity increases with the value of the target stress ($\hat{\sigma}_0$) in the contractile fibers (Figure 3d). This prediction is consistent with the experiments of Okeyo et al. [2009], who found that EKs move faster when exposed to the contraction enhancer calyculin and slower when exposed to the contraction inhibitor blebbistatin.

In addition to these key results, Barnhart et al. [2010] recently have found that crawling EKs exhibit oscillations under certain conditions. They speculate that these oscillations are caused by dynamic interactions between cell elasticity and cell-substrate adhesions. Moreover, most other types of cells, e.g., fibroblasts, crawl in a cyclic manner. Interestingly, our 1-D model oscillates for relatively small values of the hydraulic permeability or large values of the friction coefficient (Figure 4a,b). These results suggest that the oscillations are caused by delays in the feedback loops in our models, i.e., phase differences that often characterize poroelastic and frictional systems. This type of behavior is commonly encountered in feedback control systems.

Limitations. This study focuses solely on mechanical aspects of cell crawling. Biochemistry and detailed molecular mechanisms, e.g., adhesion dynamics, receptor-ligand binding, and stress fiber assembly, are not considered, although they clearly play major roles in this problem [DiMilla et al. 1991; Boulbitch et al. 2001; Schaub et al. 2007; Yam et al. 2007; Vicente-Manzanares et al. 2009]. We also do not consider some of the more detailed mechanical events, such as lamellipodial ruffling [Zhang 2009], the effects of substrate stiffness on cell speed and direction [Pelham and Wang 1997; Lo et al. 2000; Ghosh et al. 2007], and how crawling cells probe their environment [Mattila and Lappalainen 2008; Petrie et al. 2009]. These effects are beyond the scope of the present study.

Concluding remarks. Our models reproduce quite well a relatively wide range of experimental data obtained for crawling EKs. There are some discrepancies, however. A crucial unresolved issue is how the cell achieves steady state motion in two dimensions. A number of investigators have pondered this problem, with some suggesting that a gradient in actin polymerization along the leading edge is a necessary ingredient [Lee et al. 1993; Grimm et al. 2003; Rubinstein et al. 2009]. Although our 2-D crawling model includes such a gradient, it clearly is still missing something essential. One possibility is that the stress fiber along the trailing edge and the strong adhesions at the ends of the fiber are important factors. This problem remains fertile ground for future work.

A personal note

This paper is dedicated to Marie-Louise and Charles Steele. The first author (Taber) has had the privilege of knowing them since his days as a graduate student. MarieLu treated JoMMS as her "baby" and was instrumental in helping Charles establish and maintain its high standards. She was loved by all and is greatly missed. Taber learned the art of mathematical modeling from Professor Steele, who was his doctoral research advisor. Although the models presented in this paper cannot rival the extraordinarily creative and mathematically rigorous models of Professor Steele, we have striven to make them consistent with his teachings. That is, our models are based on fundamental physical principles, include (we hope) the most essential elements, and have been tested in multiple ways using experimental data. We wish him a pleasant retirement.

Acknowledgements

We thank Anders Carlsson for helpful discussions and insights regarding the biophysics of cell crawling.

References

[Adachi et al. 2009] T. Adachi, K. O. Okeyo, Y. Shitagawa, and M. Hojo, "Strain field in actin filament network in lamellipodia of migrating cells: implication for network reorganization", *J. Biomech.* **42**:3 (2009), 297–302.

[Alt and Dembo 1999] W. Alt and M. Dembo, "Cytoplasm dynamics and cell motion: two-phase flow models", *Math. Biosci.* **156**:1–2 (1999), 207–228.

[An and Fredberg 2007] S. S. An and J. J. Fredberg, "Biophysical basis for airway hyperresponsiveness", *Can. J. Physiol. Pharmacol.* **85**:7 (2007), 700–714.

[Barnhart et al. 2010] E. L. Barnhart, G. M. Allen, F. Jülicher, and J. A. Theriot, "Bipedal locomotion in crawling cells", *Biophys. J.* **98**:6 (2010), 933–942.

[Biot 1972] M. Biot, "Theory of finite deformations of porous solids", *Indiana Univ. Math. J.* **21**:7 (1972), 597–620.

[Blatz and Ko 1962] P. J. Blatz and W. L. Ko, "Application of finite elastic theory to the deformation of rubbery materials", *Trans. Soc. Rheol.* **6**:1 (1962), 223–251.

[Bossé et al. 2008] Y. Bossé, A. Sobieszek, P. D. Paré, and C. Y. Seow, "Length adaptation of airway smooth muscle", *Proc. Am. Thorac. Soc.* **5**:1 (2008), 62–67.

[Boulbitch et al. 2001] A. Boulbitch, Z. Guttenberg, and E. Sackmann, "Kinetics of membrane adhesion mediated by ligand-receptor interaction studied with a biomimetic system", *Biophys. J.* **81**:5 (2001), 2743–2751.

[Bowen 1976] R. M. Bowen, "Theory of mixtures", pp. 1–127 in *Continuum physics, III: Mixtures and EM field theories*, edited by A. C. Eringen, Academic Press, New York, 1976.

[Bray 2001] D. Bray, *Cell movements: from molecules to motility*, Garland, New York, 2001.

[Carlsson and Sept 2008] A. E. Carlsson and D. Sept, "Mathematical modeling of cell migration", *Methods Cell Biol.* **84** (2008), 911–937.

[Charras et al. 2005] G. T. Charras, J. C. Yarrow, M. A. Horton, L. Mahadevan, and T. J. Mitchison, "Non-equilibration of hydrostatic pressure in blebbing cells", *Nature* **435**:7040 (2005), 365–369.

[DiMilla et al. 1991] P. A. DiMilla, K. Barbee, and D. A. Lauffenburger, "Mathematical model for the effects of adhesion and mechanics on cell migration speed", *Biophys. J.* **60**:1 (1991), 15–37.

[Flaherty et al. 2007] B. Flaherty, J. P. McGarry, and P. E. McHugh, "Mathematical models of cell motility", *Cell Biochem. Biophys.* **49**:1 (2007), 14–28.

[Fournier et al. 2010] M. F. Fournier, R. Sauser, D. Ambrosi, J.-J. Meister, and A. B. Verkhovsky, "Force transmission in migrating cells", *J. Cell Biol.* **188**:2 (2010), 287–297.

[Friedl and Bröcker 2000] P. Friedl and E.-B. Bröcker, "The biology of cell locomotion within three-dimensional extracellular matrix", *Cell Mol. Life Sci.* **57**:1 (2000), 41–64.

[Galbraith and Sheetz 1999] C. G. Galbraith and M. P. Sheetz, "Keratocytes pull with similar forces on their dorsal and ventral surfaces", *J. Cell Biol.* **147**:6 (1999), 1313–1324.

[Ghosh et al. 2007] K. Ghosh, Z. Pan, E. Guan, S. R. Ge, Y. J. Liu, T. Nakamura, X.-D. Ren, M. Rafailovich, and R. A. F. Clark, "Cell adaptation to a physiologically relevant ECM mimic with different viscoelastic properties", *Biomater.* **28**:4 (2007), 671–679.

[Gracheva and Othmer 2004] M. E. Gracheva and H. G. Othmer, "A continuum model of motility in ameboid cells", *Bull. Math. Biol.* **66**:1 (2004), 167–193.

[Grimm et al. 2003] H. P. Grimm, A. B. Verkhovsky, A. Mogilner, and J.-J. Meister, "Analysis of actin dynamics at the leading edge of crawling cells: implications for the shape of keratocyte lamellipodia", *Eur. Biophys. J.* **32**:6 (2003), 563–577.

[Guilak et al. 2006] F. Guilak, M. A. Haider, L. A. Setton, T. A. Laursen, and F. P. T. Baaijens, "Multiphasic models of cell mechanics", pp. 84–102 in *Cytoskeletal mechanics: models and measurements*, edited by M. R. K. Mofrad and R. D. Kamm, Cambridge University Press, New York, 2006.

[Howard 2001] J. Howard, *Mechanics of motor proteins and the cytoskeleton*, Sinauer, Sunderland, MA, 2001.

[Humphrey 2008] J. D. Humphrey, "Vascular adaptation and mechanical homeostasis at tissue, cellular, and sub-cellular levels", *Cell Biochem. Biophys.* **50**:2 (2008), 53–78.

[Iwasaki and Wang 2008] T. Iwasaki and Y.-L. Wang, "Cytoplasmic force gradient in migrating adhesive cells", *Biophys. J.* **94**:5 (2008), L35–L37.

[Jurado et al. 2005] C. Jurado, J. R. Haserick, and J. Lee, "Slipping or gripping? Fluorescent speckle microscopy in fish keratocytes reveals two different mechanisms for generating a retrograde flow of actin", *Mol. Biol. Cell* **16**:2 (2005), 507–518.

[Kenyon 1976] D. E. Kenyon, "The theory of an incompressible solid-fluid mixture", *Arch. Ration. Mech. Anal.* **62**:2 (1976), 131–147.

[Keren et al. 2008] K. Keren, Z. Pincus, G. M. Allen, E. L. Barnhart, G. Marriott, A. Mogilner, and J. A. Theriot, "Mechanism of shape determination in motile cells", *Nature* **453**:7194 (2008), 475–480.

[Keren et al. 2009] K. Keren, P. T. Yam, A. Kinkhabwala, A. Mogilner, and J. A. Theriot, "Intracellular fluid flow in rapidly moving cells", *Nat. Cell Biol.* **11**:10 (2009), 1219–1224.

[Kruse et al. 2006] K. Kruse, J. F. Joanny, F. Jülicher, and J. Prost, "Contractility and retrograde flow in lamellipodium motion", *Phys. Biol.* **3**:2 (2006), 130–137.

[Kuusela and Alt 2009] E. Kuusela and W. Alt, "Continuum model of cell adhesion and migration", *J. Math. Biol.* **58**:1-2 (2009), 135–161.

[Larripa and Mogilner 2006] K. Larripa and A. Mogilner, "Transport of a 1D viscoelastic actin-myosin strip of gel as a model of a crawling cell", *Physica A* **372**:1 (2006), 113–123.

[Lee et al. 1993] J. Lee, A. Ishihara, J. A. Theriot, and K. Jacobson, "Principles of locomotion for simple-shaped cells", *Nature* **362**:6416 (1993), 167–171.

[Lo et al. 2000] C.-M. Lo, H.-B. Wang, M. Dembo, and Y.-L. Wang, "Cell movement is guided by the rigidity of the substrate", *Biophys. J.* **79**:1 (2000), 144–152.

[Loitto et al. 2009] V. M. Loitto, T. Karlsson, and K.-E. Magnusson, "Water flux in cell motility: expanding the mechanisms of membrane protrusion", *Cell Motil. Cytoskelet.* **66**:5 (2009), 237–247.

[Mattila and Lappalainen 2008] P. K. Mattila and P. Lappalainen, "Filopodia: molecular architecture and cellular functions", *Nat. Rev. Mol. Cell Biol.* **9**:6 (2008), 446–454.

[Mitchison et al. 2008] T. J. Mitchison, G. T. Charras, and L. Mahadevan, "Implications of a poroelastic cytoplasm for the dynamics of animal cell shape", *Sem. Cell Dev. Biol.* **19**:3 (2008), 215–223.

[Okeyo et al. 2009] K. O. Okeyo, T. Adachi, J. Sunaga, and M. Hojo, "Actomyosin contractility spatiotemporally regulates actin network dynamics in migrating cells", *J. Biomech.* **42**:15 (2009), 2540–2548.

[Oster and Perelson 1987] G. F. Oster and A. S. Perelson, "The physics of cell motility", *J. Cell Sci. Suppl.* **8** (1987), 35–54.

[Palecek et al. 1997] S. P. Palecek, J. C. Loftus, M. H. Ginsberg, D. A. Lauffenburger, and A. F. Horwitz, "Integrin-ligand binding properties govern cell migration speed through cell-substratum adhesiveness", *Nature* **385**:6616 (1997), 537–540.

[Pelham and Wang 1997] R. J. Pelham, Jr. and Y.-L. Wang, "Cell locomotion and focal adhesions are regulated by substrate flexibility", *Proc. Nat. Acad. Sci. USA* **94**:25 (1997), 13661–13665.

[Peskin et al. 1993] C. S. Peskin, G. M. Odell, and G. F. Oster, "Cellular motions and thermal fluctuations: the Brownian ratchet", *Biophys. J.* **65**:1 (1993), 316–324.

[Petrie et al. 2009] R. J. Petrie, A. D. Doyle, and K. M. Yamada, "Random versus directionally persistent cell migration", *Nat. Rev. Mol. Cell Biol.* **10**:8 (2009), 538–549.

[Peyton and Putnam 2005] S. R. Peyton and A. J. Putnam, "Extracellular matrix rigidity governs smooth muscle cell motility in a biphasic fashion", *J. Cell. Physiol.* **204**:1 (2005), 198–209.

[Prass et al. 2006] M. Prass, K. Jacobson, A. Mogilner, and M. Radmacher, "Direct measurement of the lamellipodial protrusive force in a migrating cell", *J. Cell Biol.* **174**:6 (2006), 767–772.

[Rodriguez et al. 1994] E. K. Rodriguez, A. Hoger, and A. D. McCulloch, "Stress-dependent finite growth in soft elastic tissues", *J. Biomech.* **27**:4 (1994), 455–467.

[Rubinstein et al. 2005] B. Rubinstein, K. Jacobson, and A. Mogilner, "Multiscale two-dimensional modeling of a motile simple-shaped cell", *Multiscale Model. Simul.* **3**:2 (2005), 413–439.

[Rubinstein et al. 2009] B. Rubinstein, M. F. Fournier, K. Jacobson, A. B. Verkhovsky, and A. Mogilner, "Actin-myosin viscoelastic flow in the keratocyte lamellipod", *Biophys. J.* **97**:7 (2009), 1853–1863.

[Schaub et al. 2007] S. Schaub, S. Bohnet, V. M. Laurent, J.-J. Meister, and A. B. Verkhovsky, "Comparative maps of motion and assembly of filamentous actin and myosin II in migrating cells", *Mol. Biol. Cell* **18**:10 (2007), 3723–3732.

[Stolarska et al. 2009] M. A. Stolarska, Y. Kim, and H. G. Othmer, "Multi-scale models of cell and tissue dynamics", *Phil. Trans. R. Soc. A* **367**:1902 (2009), 3525–3553.

[Stossel 1994] T. P. Stossel, "The machinery of cell crawling", *Sci. Am.* **271**:3 (1994), 54–63.

[Svitkina et al. 1997] T. M. Svitkina, A. B. Verkhovsky, K. M. McQuade, and G. G. Borisy, "Analysis of the actin-myosin II system in fish epidermal keratocytes: mechanism of cell body translocation", *J. Cell Biol.* **139**:2 (1997), 397–415.

[Taber 2001] L. A. Taber, "Biomechanics of cardiovascular development", *Annu. Rev. Biomed. Eng.* **3** (2001), 1–25.

[Taber 2004] L. A. Taber, *Nonlinear theory of elasticity: applications in biomechanics*, World Scientific, River Edge, NJ, 2004.

[Taber 2008] L. A. Taber, "Theoretical study of Beloussov's hyper-restoration hypothesis for mechanical regulation of morphogenesis", *Biomech. Model. Mechanobiol.* **7** (2008), 427–441.

[Verkhovsky et al. 1999] A. B. Verkhovsky, T. M. Svitkina, and G. G. Borisy, "Self-polarization and directional motility of cytoplasm", *Curr. Biol.* **9**:1 (1999), 11–20.

[Vicente-Manzanares et al. 2009] M. Vicente-Manzanares, X. F. Ma, R. S. Adelstein, and A. R. Horwitz, "Non-muscle myosin II takes centre stage in cell adhesion and migration", *Nat. Rev. Mol. Cell Biol.* **10**:11 (2009), 778–790.

[Wilson et al. 2010] C. A. Wilson, M. A. Tsuchida, G. M. Allen, E. L. Barnhart, K. T. Applegate, P. T. Yam, L. Ji, K. Keren, G. Danuser, and J. A. Theriot, "Myosin II contributes to cell-scale actin network treadmilling through network disassembly", *Nature* **465**:7296 (2010), 373–377.

[Yam et al. 2007] P. T. Yam, C. A. Wilson, L. Ji, B. Hebert, E. L. Barnhart, N. A. Dye, P. W. Wiseman, G. Danuser, and J. A. Theriot, "Actin-myosin network reorganization breaks symmetry at the cell rear to spontaneously initiate polarized cell motility", *J. Cell Biol.* **178**:7 (2007), 1207–1221.

[Yang et al. 1994] M. Yang, L. A. Taber, and E. B. Clark, "A nonlinear poroelastic model for the trabecular embryonic heart", *J. Biomech. Eng.* (*ASME*) **116**:2 (1994), 213–223.

[Young and Mitran 2010] J. Young and S. A. Mitran, "A numerical model of cellular blebbing: a volume-conserving, fluid-structure interaction model of the entire cell", *J. Biomech.* **43**:2 (2010), 210–220.

[Zhang 2009] Y.-W. Zhang, "Mechanics of membrane instability in biological cells", *Appl. Phys. Lett.* **94**:16 (2009), 163903.

[Zhu and Skalak 1988] C. Zhu and R. Skalak, "A continuum model of protrusion of pseudopod in leukocytes", *Biophys. J.* **54**:6 (1988), 1115–1137.

[Zicha et al. 2003] D. Zicha, I. M. Dobbie, M. R. Holt, J. Monypenny, D. Y. H. Soong, C. Gray, and G. A. Dunn, "Rapid actin transport during cell protrusion", *Science* **300**:5616 (2003), 142–145.

Received 19 Apr 2010. Revised 16 Sep 2010. Accepted 30 Sep 2010.

LARRY A. TABER: lat@wustl.edu
Department of Biomedical Engineering, Washington University, 1 Brookings Drive, Box 1097, St. Louis, MO 63130, United States

YUNFEI SHI: ys12@cec.wustl.edu
Department of Biomedical Engineering, Washington University, 1 Brookings Drive, Box 1097, St. Louis, MO 63130, United States

LE YANG: le@biomed.wustl.edu
Department of Biomedical Engineering, Washington University, 1 Brookings Drive, Box 1097, St. Louis, MO 63130, United States

PHILIP V. BAYLY: baylyp@seas.wustl.edu
Department of Mechanical Engineering and Materials Science, Washington University, 1 Brookings Drive, Box 1097, St. Louis, MO 63130, United States